
Sequential Unsupervised Domain Adaptation through Prototypical Distributions

Mohammad Rostami

University of Southern California
 rostamim@usc.edu

Aram Galstyan

University of Southern California
 galstyan@isi.edu

Abstract

We develop an algorithm for unsupervised domain adaptation (UDA) of a classifier from a labeled source domain to an unlabeled target domain in a sequential learning setting. UDA has been studied extensively recently but the vast majority of the existing methods consider a joint learning setting where the model is trained on the source domain and the target domain data simultaneously. We consider a more practical setting, where the model has been trained on the labeled source domain data and then needs to be adapted to the unlabeled source domain, without having access to the source domain training data. We tackle this problem by aligning the distributions of the source and the target domain in a discriminative embedding space. To overcome the challenges of learning in a sequential setting, we learn an intermediate prototypical distribution from the source labeled data and then use this distribution for knowledge transfer to the target domain. We provide theoretical justification for the proposed algorithm by showing that it optimizes an upper-bound for the expected risk in the target domain. We also conduct extensive experiments with several standard benchmarks and demonstrate the competitiveness of the proposed method compared to existing joint learning UDA algorithms.

1 Introduction

Advances in deep learning have led to significant performance improvement in a wide range of supervised learning tasks. Unfortunately, this success is largely conditioned on availability of massive labeled datasets for training deep neural networks, which may not be always feasible due to prohibitive costs [1]. A simple solution to tackle this challenge is to transfer knowledge by pre-training a neural network in a related source domain in which labeled data is available. However, pre-training is not effective when there is a domain gap between distributions of the source and the target domains. Besides, pre-training still requires target domain labeled data. Domain adaptation is a learning setting in which the goal is to leverage a source domain with labeled data to acclimate a deep neural network to generalize well in a target domain in which only unlabeled data is accessible [2].

An effective approach for domain adaptation is to align distributions of both domains by mapping data into a latent domain-invariant space [3, 4]. As a result, a classifier that is trained using the source labeled data features in this space will generalize well in the target domain. Recent domain adaptation methods model this latent space as the output of a shared deep encoder. The encoder network is trained such that the source and the target domains share a similar distribution in its output. This training procedure have been implemented using either adversarial learning [5–9] or by directly minimizing the distance between the two distributions in the embedding [10–13, 13–15]. Adversarial learning [16] has been used to extract features that are maximally discriminative in the source domain and at the same as indistinguishable as possible in the target domain. As a result, the distributions are aligned indirectly. Despite being effective, adversarial learning often requires delicate optimization initialization, architecture engineering, and careful selection of hyper-parameters to be stable [17].

Adversarial learning can also suffer from mode collapse [18]. In contrast, choosing the proper probability distribution metric is the challenge for direct probability matching.

Most existing unsupervised domain adaptation (UDA) algorithms consider a joint learning setting, where the model is trained using both the target domain unlabeled data and the source domain labeled data. In this paper, we consider a more realistic sequential learning scenario where the original training data is not necessarily available during the adaptation. Instead, we assume that a model that is trained on the source domain is given and the goal is to adapt this model to generalize well in the target domain using solely the target domain unlabeled data. This setting can be considered as an improvement over using an off-the-shelf pre-trained model when unlabeled data in a source domain is available. It also relaxes the necessity of sharing training data between the two domains.

Contributions: our main contribution is to develop a sequential UDA algorithm which is based on learning a parametric prototypical distribution for the source domain data distribution in the shared embedding space. This prototypical distribution is used to align the source and the target distributions. We approximate this multimodal distribution using a Gaussian mixture model (GMM). In order to adapt the model to work well the target domain, we draw samples from this prototypical distribution and enforce the target domain to share the same prototypical distribution in the embedding space.

We also provide a theoretical justification for the proposed algorithm, by establishing an upper bound for the expected risk in the target domain, and demonstrating that the proposed algorithm minimizes this bound. Finally, we conduct extensive experiments and observe that the proposed approach compares favorably with state-of-the-art joint learning UDA methods.

2 Background and Related Work

Several discrepancy measures have been used to align two distributions to address UDA. A group of methods match the first-order and the second order statistics of the source and the target domains. This includes methods that use the Maximum Mean Discrepancy (MMD) [10, 12] and correlation alignment [19]. A more effective approach is to use a probability distance that captures differences in higher order statistics. The Wasserstein distance (WD) [20, 21] is such an example that is also a suitable metric for deep learning due to having non-vanishing gradients. This property is helpful because deep learning optimization problems are usually solved using the first-order gradient-based optimization methods. Damodaran et al. [21] use the WD for domain alignment in a UDA setting which leads to considerable performance improvement compared to methods [10, 19] that rely on matching lower order statistics. In this work, we rely on the sliced Wasserstein distance (SWD) variant of WD [22] for domain alignment. Compared to WD, SWD can be computed more efficiently.

Most existing UDA methods use a strong assumption. It is assumed that the source and the target domain data are accessible simultaneously and the model is trained jointly on two datasets. Since pre-trained models are currently available, it is more practical to adapt them using only the target domain data. By doing so, we can also address UDA when the source domain data is Private. This learning setting for domain adaptation has been explored for non-deep models [23–25]. However, these works address sequential UDA when the input distribution can be estimated with a parametric distribution and the base models have a small number of parameters. As a result, it is not trivial to extend the above works for the end-to-end training of deep neural networks. We use the notion of prototypical distribution to align two distributions when the base model is a deep neural network.

Quite recently, UDA has been addressed through the idea of cross-domain alignment of the class prototypes. The core assumption is that the data points that belong to each class form a single cluster in the shared embedding space. Each class then can be represented by a single prototype (centroid). Solving UDA then would reduce to aligning the prototypes across the domains by minimizing a loss function that measures the distance between the prototype pairs [26, 27]. Pan et al. [26] measure the distance between the prototypes in a reproducing kernel Hilbert space (RKHS) and use KL-divergence to align the sample-based distributions. Chen et al. [27] measure the prototype-level distance in ℓ_2 -norm and use adversarial learning to align the distributions. We base our work on the above mentioned assumption but rather learning only the prototypes, we learn a prototypical distribution in the embedding space. This distribution is a multimodal distribution that encodes the knowledge gained from supervised learning in the source domain. We develop an algorithm for sequential UDA by enforcing the target domain to share this distribution in the embedding space.

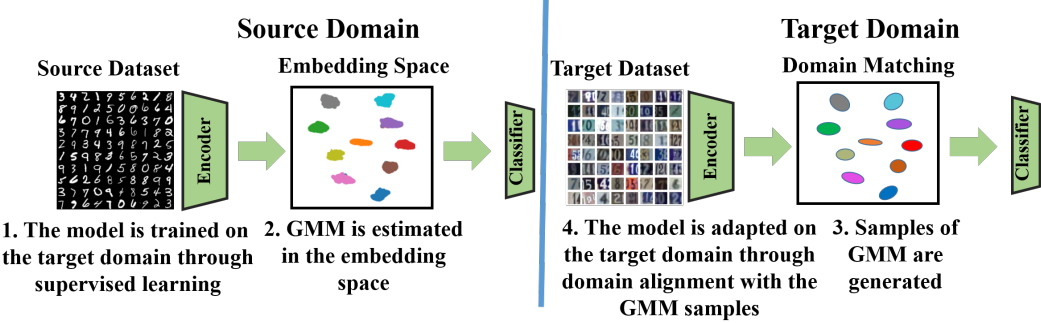


Figure 1: Architecture of the proposed unsupervised domain adaptation framework.

3 Problem Statement

Consider a source domain \mathcal{S} which consists of the distribution $p_S(\mathbf{x})$ and the labeling function $f(\cdot) : \mathbb{R}^d \rightarrow \mathcal{Y} \subset \mathbb{R}^k$. Given a family of parametric functions $f_\theta : \mathbb{R}^d \rightarrow \mathcal{Y}$, e.g., a deep neural network with learnable parameter θ , our goal is to solve for an optimal model with minimum expected risk, i.e., $\mathbb{E}_{\mathbf{x}^s \sim p_S(\mathbf{x})}(\mathcal{L}(f(\mathbf{x}^s), f_\theta(\mathbf{x}^s)))$, where $\mathcal{L}(\cdot)$ is a proper loss function. To this end, we are given a labeled dataset $\mathcal{D}_S = (\mathbf{X}_S, \mathbf{Y}_S)$, with $\mathbf{X}_S = [\mathbf{x}_1^s, \dots, \mathbf{x}_N^s] \in \mathcal{X} \subset \mathbb{R}^{d \times N}$ and $\mathbf{Y}_S = [\mathbf{y}_1^s, \dots, \mathbf{y}_N^s] \in \mathcal{Y} \subset \mathbb{R}^{k \times N}$, where the data points are drawn i.i.d. $\mathbf{x}_i^s \sim p_S(\mathbf{x})$. Given a sufficiently large enough number of labeled data points, we can solve for the optimal parameters using the standard empirical risk minimization (ERM): $\hat{\theta} = \arg \min_{\theta} \hat{e}_{\theta}(\mathbf{X}_S, \mathbf{Y}_S, \mathcal{L}) = \arg \min_{\theta} \sum_i \mathcal{L}(f_\theta(\mathbf{x}_i^s), \mathbf{y}_i^s)$, as a surrogate for the true risk. Consider that we are also given an unlabeled dataset $\mathcal{D}_T = (\mathbf{X}_T)$ in a target domain with $\mathbf{X}_T = [\mathbf{x}_1^t, \dots, \mathbf{x}_M^t] \in \mathbb{R}^{d \times M}$ and $\mathbf{x}_i^t \sim p_T(\mathbf{x})$. As a result, using ERM is not feasible in the target domain. We know a priori that the two domains share the same classes but despite this strong relation, distributional discrepancy exists between the two domains, i.e. $p_S \neq p_T$ which leads to poor generalization of $f_{\hat{\theta}}$ in the target domain. Our goal is to adapt the classifier $f_{\hat{\theta}}$ using solely the dataset \mathcal{D}_T such that it generalizes well in the target domain (see Figure 1).

In order to circumvent the challenge of distributional gap between the two domains, we can decompose the mapping $f_\theta(\cdot)$ into a deep encoder $\phi_v(\cdot) : \mathcal{X} \rightarrow \mathcal{Z} \subset \mathbb{R}^p$ and a classifier $h_w(\cdot) : \mathcal{Z} \rightarrow \mathcal{Y}$ such that $f_\theta = h_w \circ \phi_v$, where $\theta = (\mathbf{w}, \mathbf{v})$. Here, \mathcal{Z} denotes an intermediate embedding space between the input space and the label space in which we assume that the classes have become geometrically separable. Given $\hat{\theta}$ and \mathcal{D}_T , if we adapt ϕ_v such that the discrepancy between the source and target distributions, i.e., the distance between $\phi(p_S(\mathbf{x}^s))$ and $\phi(p_T(\mathbf{x}^t))$, is minimized in the embedding space (making the embedding domain agnostic), then the classifier h_w will generalize well on the target domain. Many prior classic UDA algorithms use this strategy but implement it by assuming that \mathcal{D}_S is always accessible. This makes computing the distance between the distributions $\phi(p_S(\mathbf{x}^s))$ and $\phi(p_T(\mathbf{x}^t))$ simple and hence UDA reduces to selecting a proper probability distribution metric and then solving a typical deep learning minimization problem [10, 12, 21, 20, 21]. The major challenge in the sequential UDA setting is that the term $\phi(p_S(\mathbf{x}^s))$ cannot be computed directly.

4 Proposed Solution

We propose to solve the challenge of sequential UDA through aligning the source and the target distribution via an intermediate prototypical distribution in the embedding space. We set a softmax function at the output of the encoder just before passing data representations into the classifier sub-network. As a result, the classifier can be assumed as a maximum *a posteriori* (MAP) estimator which assigns a membership probability distribution to any given data point. This means that when an optimal model is trained for the source domain, the encoder would transform the source distribution into a multi-modal distribution $p_J(\mathbf{z})$ with k components in the embedding space (see Figure 1, right). This occurs because the classes should become separable in the embedding space as the result of learning. This is a prototypical distribution in which each distribution mode would capture one of the classes. The mean for each mode can be considered as the class prototype in the previous

works [26, 27]. If we update the model such that the prototypical distribution remains stable in the target domain after adaptation, then the classifier would generalize well in the target domain.

The empirical version of the prototypical distribution is encoded by the source data samples $\{(\phi_v(\mathbf{x}_i^s), \mathbf{y}_i^s)\}_{i=1}^N$. We consider the distribution $p_J(\mathbf{z})$ to be a GMM with k components:

$$p_J(\mathbf{z}) = \sum_{j=1}^k \alpha_j \mathcal{N}(\mathbf{z} | \boldsymbol{\mu}_j, \boldsymbol{\Sigma}_j), \quad (1)$$

where α_j denote mixture weights, i.e., prior probability for each class, $\boldsymbol{\mu}_j$ and $\boldsymbol{\Sigma}_j$ denote the mean and co-variance for each component. Since we have labeled data points, we can compute the GMM parameters using MAP estimates. Let \mathcal{S}_j denote the support set for class j in the training dataset, i.e., $\mathcal{S}_j = \{(\mathbf{x}_i^s, \mathbf{y}_i^s) \in \mathcal{D}_S \mid \arg \max \mathbf{y}_i^s = j\}$. Then, the MAP estimate for the parameters would be:

$$\hat{\alpha}_j = \frac{|\mathcal{S}_j|}{N}, \quad \hat{\boldsymbol{\mu}}_j = \sum_{(\mathbf{x}_i^s, \mathbf{y}_i^s) \in \mathcal{S}_j} \frac{1}{|\mathcal{S}_j|} \phi_v(\mathbf{x}_i^s), \quad \hat{\boldsymbol{\Sigma}}_j = \sum_{(\mathbf{x}_i^s, \mathbf{y}_i^s) \in \mathcal{S}_j} \frac{1}{|\mathcal{S}_j|} (\phi_v(\mathbf{x}_i^s) - \hat{\boldsymbol{\mu}}_j)^\top (\phi_v(\mathbf{x}_i^s) - \hat{\boldsymbol{\mu}}_j). \quad (2)$$

Our major idea is to use this prototypical distributional estimate to circumvent the major challenge of sequential UDA. In order to adapt the model to work well for the target domain, we update the model such that the encoder matches the target distribution into the prototypical distribution in the embedding space. To this end, we can draw samples from the prototypical distributional estimate and generate a labeled pseudo-dataset: $\hat{\mathcal{D}} = (\mathbf{Z}_P, \mathbf{Y}_P)$, where $\mathbf{Z}_P = [\mathbf{z}_1^p, \dots, \mathbf{z}_{N_p}^p] \in \mathbb{R}^{p \times N_p}$, $\mathbf{Y}_P = [\mathbf{y}_1^p, \dots, \mathbf{y}_{N_p}^p] \in \mathbb{R}^{k \times N_p}$, $\mathbf{z}_i^p \sim \hat{p}_J(\mathbf{z})$, and the labels are ascribed according to the classifier sub-network prediction. The sequential UDA problem then reduces to the following problem:

$$\min_{\mathbf{v}, \mathbf{w}} \sum_{i=1}^N \mathcal{L}(h_{\mathbf{w}}(\mathbf{z}_i^p), \mathbf{y}_i^p) + \lambda D(\phi_v(p_{\mathcal{T}}(\mathbf{X}_{\mathcal{T}})), \hat{p}_J(\mathbf{Z}_P)), \quad (3)$$

where $D(\cdot, \cdot)$ denotes a probability metric to measure the discrepancy measure between two distributions, and λ is a trade-off parameter between the two terms (see Figure 1, left).

Algorithm 1 SDAUP (λ, ITR)

- 1: **Initial Training:**
- 2: **Input:** source dataset $\mathcal{D}_S = (\mathbf{X}_S, \mathbf{Y}_S)$,
- 3: **Training on Source Domain:**
- 4: $\hat{\theta}_0 = (\hat{w}_0, \hat{v}_0) = \arg \min_{\theta} \sum_i \mathcal{L}(f_{\theta}(\mathbf{x}_i^s), \mathbf{y}_i^s)$
- 5: **Prototypical Distribution Estimation:**
- 6: Use Eq. (2) and estimate $\alpha_j, \boldsymbol{\mu}_j$, and $\boldsymbol{\Sigma}_j$
- 7: **Model Adaptation:**
- 8: **Input:** target dataset $\mathcal{D}_{\mathcal{T}} = (\mathbf{X}_{\mathcal{T}})$
- 9: **Pseudo-Dataset Generation:**
- 10: $\hat{\mathcal{D}}_P = (\mathbf{Z}_P, \mathbf{Y}_P) = ([\mathbf{z}_1^p, \dots, \mathbf{z}_{N_p}^p], [\mathbf{y}_1^p, \dots, \mathbf{y}_{N_p}^p])$, where:
- 11: $\mathbf{z}_i^p \sim \hat{p}_J(\mathbf{z}), 1 \leq i \leq N_p$
- 12: $\mathbf{y}_i^p = \arg \max_j \{h_{\hat{w}_0}(\mathbf{z}_i^p)\}$
- 13: **for** $itr = 1, \dots, ITR$ **do**
- 14: draw data batches from $\hat{\mathcal{D}}_{\mathcal{T}}$ and $\hat{\mathcal{D}}_P$
- 15: Update the model by solving Eq. (3)
- 17: **end for**

ure 1, respectively.

5 Theoretical Analysis

We demonstrate that our algorithm optimizes an upper-bound for the target domain expected risk. We treat the embedding space as the hypothesis space within standard PAC-learning in our analysis

and consider the hypothesis class to be the set of classifier sub-networks $\mathcal{H} = \{h_{\mathbf{w}}(\cdot) | h_{\mathbf{w}}(\cdot) : \mathcal{Z} \rightarrow \mathbb{R}^k, \mathbf{w} \in \mathbb{R}^V\}$. We denote the observed risk on the source and the target domains by $e_{\mathcal{S}}$ and $e_{\mathcal{T}}$, respectively. Also, let $\hat{\mu}_{\mathcal{S}} = \frac{1}{N} \sum_{n=1}^N \delta(\phi_{\mathbf{v}}(\mathbf{x}_n^s))$ and $\hat{\mu}_{\mathcal{T}} = \frac{1}{M} \sum_{m=1}^M \delta(\phi_{\mathbf{v}}(\mathbf{x}_m^t))$ denote the empirical source and the empirical target distributions in the embedding space, computable from the training data representations. Similarly, let $\hat{\mu}_{\mathcal{P}} = \frac{1}{N_p} \sum_{q=1}^{N_p} \delta(\mathbf{z}_n^q)$ denote the empirical prototypical distribution. Moreover, let $h_{\mathbf{w}^*}$ denote the optimal model that minimizes the combined source and target risks $e_{\mathcal{C}}(\mathbf{w}^*)$, i.e. $\mathbf{w}^* = \arg \min_{\mathbf{w}} e_{\mathcal{C}}(\mathbf{w}) = \arg \min_{\mathbf{w}} \{e_{\mathcal{S}} + e_{\mathcal{T}}\}$. In the presence of enough labeled target domain data, this is the best joint model that can be learned. Finally, let $\tau = \mathbb{E}_{\mathbf{z} \sim p_{\mathcal{J}}(\mathbf{z})} (\mathcal{L}(h(\mathbf{z}), h_{\hat{\mathbf{w}}_0}(\mathbf{z}))$ denotes the expected risk of the optimal model that is trained using the source domain data on the generated pseudo-dataset using the GMM distribution. This is the baseline performance of the source-trained model in the target domain.

Theorem 1: Consider that we generate a pseudo-dataset using the prototypical distribution and update the model for sequential UDA using algorithm 1. Then, the following holds:

$$e_{\mathcal{T}} \leq e_{\mathcal{S}} + W(\hat{\mu}_{\mathcal{S}}, \hat{\mu}_{\mathcal{P}}) + W(\hat{\mu}_{\mathcal{T}}, \hat{\mu}_{\mathcal{P}}) + (1 - \tau) + e_{\mathcal{C}'}(\mathbf{w}^*) + \sqrt{(2 \log(\frac{1}{\xi})/\zeta)} (\sqrt{\frac{1}{N}} + \sqrt{\frac{1}{M}} + 2\sqrt{\frac{1}{N_p}}), \quad (4)$$

where $W(\cdot, \cdot)$ denotes the WD distance and ξ is a constant which depends on $\mathcal{L}(\cdot)$.

Proof: due to the space constraint, the complete proof is included in the Appendices.

Theorem 1 demonstrate why our algorithm can adapt the model that is trained using the source domain to generalize well on the target domain. We can see that SDAUP algorithm minimizes the upperbound of the target domain risk as given in Eq. (4). We minimize the source risk $e_{\mathcal{S}}$ through the initial training on the source domain. We minimize the second term in the upperbound of Eq. (4) by intentionally fitting a GMM distribution on the source domain distribution in the embedding. We note that this is only feasible if the source domain distribution can be fit well with a GMM distribution. The third term is minimized because it is one of the terms in the objective function of Eq. (2). The last term in Eq. (2) is a constant term that merely states that in order to train a good model, we need sufficiently large source and target datasets and also generate a large pseudo-dataset. The fourth and fifth terms state conditions under which our algorithm would work. The term $(1 - \tau)$ is an important term and SDAUP does not minimize. However, this term is small if the source-trained model can initially generalize in target domain to some extent. This is quite intuitive because we don't expect positive knowledge transfer between two unrelated domains. Similarly, the term $e_{\mathcal{C}'}(\mathbf{w}^*)$ will be minimal if the domains are related, i.e., share the same classes, and in presence of the target labeled data, the base model can be trained to work well on both domains, i.e., aligning the distributions in the embedding is possible. Hence, assuming related domains, SDAUP minimizes all the remaining terms in Eq. (4), which would result in small true risk on the target domain.

6 Experimental Validation

We compare our algorithm against several recently developed UDA algorithms using benchmark UDA tasks. In order to demonstrate effectiveness of our algorithm, we consider different UDA tasks in terms of difficulty and the base network structure. Our implemented code is available at <https://github.com/mrostami1366/SequentialUDA>.

6.1 Experimental Setup

Digit tasks: MNIST (\mathcal{M}), USPS (\mathcal{U}), and Street View House Numbers, i.e., SVHN (\mathcal{S}), datasets are used as three domains. Following the literature, we report performance on three UDA tasks defined among these datasets: $\mathcal{M} \rightarrow \mathcal{U}$, $\mathcal{U} \rightarrow \mathcal{M}$, and $\mathcal{S} \rightarrow \mathcal{M}$.

Office-31 Detest: this dataset is a visual recognition dataset with a total of 4,652 images which are categorized into ten classes in three distinct domains: Amazon (\mathcal{A}), Webcam (\mathcal{W}) and DSLR (\mathcal{D}). We report performance the six pair-wise definable UDA tasks.

ImageCLEF-DA Dataset: this image classification dataset is a generated using the 12 shared classes between the Caltech-256 (\mathcal{C}), the ILSVRC 2012 (\mathcal{I}), and the Pascal VOC 2012 (\mathcal{P}) visual recognition datasets. We perform experiments on the six possible UDA tasks.

Office-Home Dataset: this dataset is a more challenging object recognition dataset with a total of 15,500 images in office and home settings, grouped in 65 classes from 4 domains with large gap: Artistic images (A), Clip Art (C), Product images (P), and Real-World images (R).

VisDA-2017: the goal for this dataset is to train a model on a synthetic domain and adapt it to work well on real natural images. The synthetic images are generated by renderings of 3D models from different angles and with different lightning conditions across 12 classes.

We use the standard precedent in the UDA literature. We use the VGG16 network as the base model for the digit recognition tasks. The network is initialized with random weights. We use the ResNet-50 network which is pre-trained on the ImageNet dataset as the backbone of the network for the rest of the tasks. We use standard cross validation to tune the hyper-parameter λ . We report the average classification rate and standard deviation based on ten runs for each UDA task. We train the base model using the source labeled data. We report the performance of this model on the target domain as a baseline. Then we adapt the model using the target unlabeled data using SDAUP algorithm and report the performance of SDAUP. Our work is the first work within sequential UDA setting. Hence, we compare our results against the existing UDA algorithms that use joint training. In our comparison, we include both pioneer and recent works to be representative. We include methods that are based on adversarial learning: GtA [6], DANN [29], SymNets [8] ADDA [30], MADA [7], and CDAN [9]. We have also included methods based on direct distribution matching that are more similar to our approach: DAN [10], DRCN [31], RevGrad [11], CAN [13], JAN [12], DACAD [32], and JDDA [33]. For each dataset, we include results of these works if the original paper have used that dataset. For more details on the experimental setup, please refer to the Appendices.

6.2 Results

Results for the digit recognition tasks are reported in Table 1. In our Tables, bold font denotes best performance and boxed text with italic font denotes the second best performances. Despite sequential training, SDAUP outperforms the other methods in two of the tasks. We note that CyCADA and JDDA methods lead to competitive results for these tasks. This maybe because CyCADA use generative pixel-level adaptation and JDDA uses an instance-Based discriminative loss. Both approaches would lead to class clusters that are highly separable in the embedding space, i.e., class clusters are distant, and hence are robust with respect to domain shift. SDAUP leads to strong results because stabilizing the prototypical distribution for both domain would also mitigate the effect of domain shift.

Table 2 summarizes the results for Office-31 dataset. We see in two of the tasks SDAUP lead to the best results. Note, however, it seems there is no clear winner for this dataset. It is reported that some labels in this dataset are noisy and some images contain objects that belong to other classes [34]. SDAUP and other methods distribution matching methods are vulnerable with respect to label pollution which makes aligning the distributions class-conditionally more challenging.

Results for UDA tasks of the ImageCLEF-DA dataset are reported in Table 3. We see that SDAUP leads to significant performance boost over the prior methods for this dataset. the Caltech-256, the ILSVRC 2012, and the Pascal VOC 2012 datasets have the equal size and are balanced in each class. As a result, matching the source and the target distributions to the same prototypical multi-modal distribution is more meaningful and straight forward for this dataset.

We have reported results for the Office-Home in Table 4. SymNets has the best result for this dataset. This maybe because SymNets uses a two-level training procedure that aligns two distributions in terms of features and classification categories. This class-conditional alignment can be particularly helpful when the gap between the two domains is large, as it is the case for the Office-Home dataset. However, we note that SDAUP leads to relatively close competitive performance for this dataset.

Results for VisDA task is presented Table 5. We observe a significant boost for VisDA task. From Tables 1–5, we conclude that there is no single UDA method with best performance on all the tasks. This occurs due to diversity of the tasks in terms of difficulty, domain gap, dataset size, etc. However, our we observe SDAUP works reasonably well on all the UDA tasks with state-of-the-art performance on many of the tasks, despite being a sequential UDA approach which assumes a more challenging and a more restrictive setting. These results demonstrate that although our motivation was to address sequential learning, SDAUP can also be used in a competitive joint training UDA algorithm.

| Method | $\mathcal{M} \rightarrow \mathcal{U}$ | $\mathcal{U} \rightarrow \mathcal{M}$ | $\mathcal{S} \rightarrow \mathcal{M}$ | Method | $\mathcal{M} \rightarrow \mathcal{U}$ | $\mathcal{U} \rightarrow \mathcal{M}$ | $\mathcal{S} \rightarrow \mathcal{M}$ |
|--------------|---------------------------------------|---------------------------------------|---------------------------------------|-------------|---------------------------------------|---------------------------------------|---------------------------------------|
| GtA [6] | 92.8 \pm 0.9 | 90.8 \pm 1.3 | 92.4 \pm 0.9 | CDAN [9] | 93.9 | 96.9 | 88.5 |
| CoGAN [35] | 91.2 \pm 0.8 | 89.1 \pm 0.8 | - | FADA [36] | 89.1 | 81.1 | 72.8 |
| ADDA [30] | 89.4 \pm 0.2 | 90.1 \pm 0.8 | 76.0 \pm 1.8 | CyCADA [37] | 95.6 \pm 0.2 | 96.5 \pm 0.1 | 90.4 \pm 0.4 |
| RevGrad [11] | 77.1 \pm 1.8 | 73.0 \pm 2.0 | 73.9 | JDDA [33] | - | 97.0 \pm 0.2 | 93.1 \pm 0.2 |
| DRCN [31] | 91.8 \pm 0.1 | 73.7 \pm 0.4 | 82.0 \pm 0.2 | OPDA [20] | 70.0 | 60.2 | - |
| DACAD [32] | 92.4 \pm 1.2 | 91.1 \pm 0.3 | 80.0 \pm 1.2 | MML [38] | 77.9 | 60.5 | 62.9 |
| Source Only | 90.1 \pm 2.6 | 80.2 \pm 5.7 | 67.3 \pm 2.6 | Ours | 96.2 \pm 0.5 | 98.2 \pm 0.2 | 92.6 \pm 1.0 |

Table 1: Classification accuracy for UDA tasks between MINIST, USPS, and SVHN datasets.

| Method | $\mathcal{A} \rightarrow \mathcal{W}$ | $\mathcal{D} \rightarrow \mathcal{W}$ | $\mathcal{W} \rightarrow \mathcal{D}$ | $\mathcal{A} \rightarrow \mathcal{D}$ | $\mathcal{D} \rightarrow \mathcal{A}$ | $\mathcal{W} \rightarrow \mathcal{A}$ |
|-----------------|---------------------------------------|---------------------------------------|---------------------------------------|---------------------------------------|---------------------------------------|---------------------------------------|
| Source Only [5] | 68.4 \pm 0.2 | 96.7 \pm 0.1 | 99.3 \pm 0.1 | 68.9 \pm 0.2 | 62.5 \pm 0.3 | 60.7 \pm 0.3 |
| GtA [6] | 89.5 \pm 0.5 | 97.9 \pm 0.3 | 99.8 \pm 0.4 | 87.7 \pm 0.5 | 72.8 \pm 0.3 | 71.4 \pm 0.4 |
| DANN [29] | 82.0 \pm 0.4 | 96.9 \pm 0.2 | 99.1 \pm 0.1 | 79.7 \pm 0.4 | 68.2 \pm 0.4 | 67.4 \pm 0.5 |
| ADDA [30] | 86.2 \pm 0.5 | 96.2 \pm 0.3 | 98.4 \pm 0.3 | 77.8 \pm 0.3 | 69.5 \pm 0.4 | 68.9 \pm 0.5 |
| SymNets [8] | 90.8 \pm 0.1 | 98.8 \pm 0.3 | 100.0 \pm 0.0 | 93.9 \pm 0.5 | 74.6 \pm 0.6 | 72.5 \pm 0.5 |
| MADA [7] | 82.0 \pm 0.4 | 96.9 \pm 0.2 | 99.1 \pm 0.1 | 79.7 \pm 0.4 | 68.2 \pm 0.4 | 67.4 \pm 0.5 |
| CDAN [9] | 93.1 \pm 0.2 | 98.2 \pm 0.2 | 100.0 \pm 0.0 | 89.8 \pm 0.3 | 70.1 \pm 0.4 | 68.0 \pm 0.4 |
| DAN [10] | 80.5 \pm 0.4 | 97.1 \pm 0.2 | 99.6 \pm 0.1 | 78.6 \pm 0.2 | 63.6 \pm 0.3 | 62.8 \pm 0.2 |
| DRCN [31] | 72.6 \pm 0.3 | 96.4 \pm 0.1 | 99.2 \pm 0.3 | 67.1 \pm 0.3 | 56.0 \pm 0.5 | 72.6 \pm 0.3 |
| RevGrad [11] | 82.0 \pm 0.4 | 96.9 \pm 0.2 | 99.1 \pm 0.1 | 79.7 \pm 0.4 | 68.2 \pm 0.4 | 67.4 \pm 0.5 |
| CAN [13] | 94.5 \pm 0.3 | 99.1 \pm 0.2 | 99.8 \pm 0.2 | 95.0 \pm 0.3 | 78.0 \pm 0.3 | 77.0 \pm 0.3 |
| JAN [12] | 85.4 \pm 0.3 | 97.4 \pm 0.2 | 99.8 \pm 0.2 | 84.7 \pm 0.3 | 68.6 \pm 0.3 | 70.0 \pm 0.4 |
| JDDA [33] | 82.6 \pm 0.4 | 95.2 \pm 0.2 | 99.7 \pm 0.0 | 79.8 \pm 0.1 | 57.4 \pm 0.0 | 66.7 \pm 0.2 |
| Ours | 97.8 \pm 2.1 | 95.6 \pm 0.5 | 99.1 \pm 0.3 | 97.8 \pm 1.7 | 68.2 \pm 4.5 | 71.7 \pm 3.6 |

Table 2: Classification accuracy for UDA tasks for Office-31 dataset.

| Method | $\mathcal{I} \rightarrow \mathcal{P}$ | $\mathcal{P} \rightarrow \mathcal{I}$ | $\mathcal{I} \rightarrow \mathcal{C}$ | $\mathcal{C} \rightarrow \mathcal{I}$ | $\mathcal{C} \rightarrow \mathcal{P}$ | $\mathcal{P} \rightarrow \mathcal{C}$ |
|-----------------|---------------------------------------|---------------------------------------|---------------------------------------|---------------------------------------|---------------------------------------|---------------------------------------|
| Source Only [5] | 74.8 \pm 0.3 | 83.9 \pm 0.1 | 91.5 \pm 0.3 | 78.0 \pm 0.2 | 65.5 \pm 0.3 | 91.2 \pm 0.3 |
| DANN [29] | 82.0 \pm 0.4 | 96.9 \pm 0.2 | 99.1 \pm 0.1 | 79.7 \pm 0.4 | 68.2 \pm 0.4 | 67.4 \pm 0.5 |
| SymNets [8] | 80.2 \pm 0.3 | 93.6 \pm 0.2 | 97.0 \pm 0.3 | 93.4 \pm 0.3 | 78.7 \pm 0.3 | 96.4 \pm 0.1 |
| MADA [7] | 75.0 \pm 0.3 | 87.9 \pm 0.2 | 96.0 \pm 0.3 | 88.8 \pm 0.3 | 75.2 \pm 0.2 | 92.2 \pm 0.3 |
| CDAN [9] | 76.7 \pm 0.3 | 90.6 \pm 0.3 | 97.0 \pm 0.4 | 90.5 \pm 0.4 | 74.5 \pm 0.3 | 93.5 \pm 0.4 |
| DAN [10] | 74.5 \pm 0.4 | 82.2 \pm 0.2 | 92.8 \pm 0.2 | 86.3 \pm 0.4 | 69.2 \pm 0.4 | 89.8 \pm 0.4 |
| RevGrad [11] | 75.0 \pm 0.6 | 86.0 \pm 0.3 | 96.2 \pm 0.4 | 87.0 \pm 0.5 | 74.3 \pm 0.5 | 91.5 \pm 0.6 |
| JAN [12] | 76.8 \pm 0.4 | 88.0 \pm 0.2 | 94.7 \pm 0.2 | 89.5 \pm 0.3 | 74.2 \pm 0.3 | 91.7 \pm 0.3 |
| Ours | 88.7 \pm 1.2 | 99.5 \pm 0.2 | 100 \pm 0.0 | 94.9 \pm 0.3 | 88.8 \pm 0.9 | 99.8 \pm 0.0 |

Table 3: Classification accuracy for UDA tasks for ImageCLEF-DA dataset.

| Method | A \rightarrow C | A \rightarrow P | A \rightarrow R | C \rightarrow A | C \rightarrow P | C \rightarrow R | P \rightarrow A | P \rightarrow C | P \rightarrow R | R \rightarrow A | R \rightarrow C | R \rightarrow P |
|-----------------|-------------------|-------------------|-------------------|-------------------|-------------------|-------------------|-------------------|-------------------|-------------------|-------------------|-------------------|-------------------|
| Source Only [5] | 34.9 | 50.0 | 58.0 | 37.4 | 41.9 | 46.2 | 38.5 | 31.2 | 60.4 | 53.9 | 41.2 | 59.9 |
| DANN [29] | 45.6 | 59.3 | 70.1 | 47.0 | 58.5 | 60.9 | 46.1 | 43.7 | 68.5 | 63.2 | 51.8 | 76.8 |
| SymNets [8] | 47.7 | 72.9 | 78.5 | 64.2 | 71.3 | 74.2 | 64.2 | 48.8 | 79.5 | 74.5 | 52.6 | 82.7 |
| CDAN [9] | 49.0 | 69.3 | 74.5 | 54.4 | 66.0 | 68.4 | 55.6 | 48.3 | 75.9 | 68.4 | 55.4 | 80.5 |
| DAN [10] | 43.6 | 57.0 | 67.9 | 45.8 | 56.5 | 60.4 | 44.0 | 43.6 | 67.7 | 63.1 | 51.5 | 74.3 |
| JAN [12] | 45.9 | 61.2 | 68.9 | 50.4 | 59.7 | 61.0 | 45.8 | 43.4 | 70.3 | 63.9 | 52.4 | 76.8 |
| DJT [21] | 39.7 | 50.4 | 62.4 | 39.5 | 54.3 | 53.1 | 36.7 | 39.2 | 63.5 | 52.2 | 45.4 | 70.4 |
| Ours | 49.3 | 70.5 | 75.8 | 53.5 | 66.2 | 67.6 | 51.1 | 45.6 | 73.8 | 64.4 | 53.2 | 77.6 |

Table 4: Classification accuracy for UDA tasks of Office-Home dataset.

6.3 Analysis

To provide a better intuition, we have used UMAP [41] visualization tool to reduce the dimension of the data representations in the embedding space to two for 2D visualization. Figure 2 represents the testing splits of the source and the target domains and samples of the prototypical for the $\mathcal{S} \rightarrow \mathcal{M}$

| Task | JAN [12] | DJT [21] | GtA [6] | SimNet [39] | CDAN [9] | MCD [40] | Ours |
|------------|----------|----------|---------|-------------|----------|----------|-------------------|
| Syn.→Real. | 61.6 | 66.9 | 69.5 | 69.6 | 70.0 | 71.9 | 76.9 ± 0.7 |

Table 5: Classification accuracy for the VisDA UDA task.

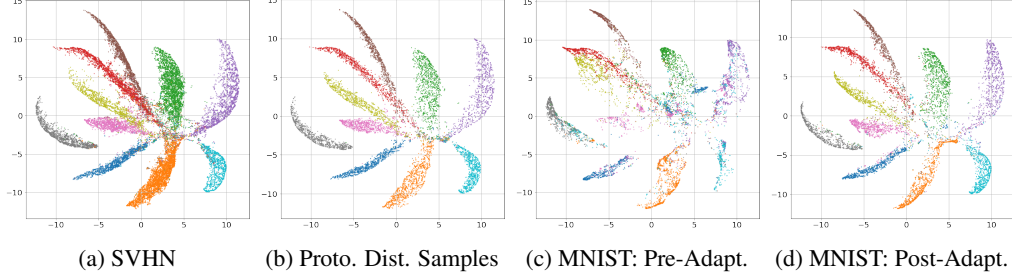


Figure 2: UMAP visualization for the $\mathcal{S} \rightarrow \mathcal{M}$ task: (a) the source domain testing split, (b) the prototypical distribution samples, (c) the target domain testing split prior to adaptation, and (d) post adaptation. (Best viewed in color).

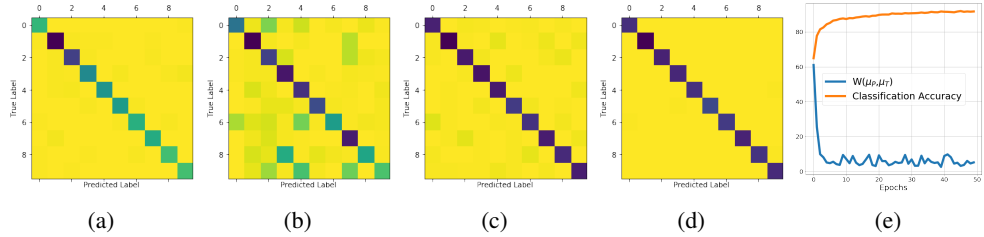


Figure 3: Confusion matrices for the $\mathcal{S} \rightarrow \mathcal{M}$ task: (a) the source domain (b) the target domain prior to adaptation, (c) the target domain after adaptation, (d) the cross-domain distribution & the test error vs learning iterations. (Best viewed enlarged on screen and in color).

digit recognition task. In this figure, each point represents one data point and each color represents one of the digit classes. Comparing Figures 2a and 2b, we can see that GMM prototypical distribution approximates the source domain distribution reasonably well. Figure 2c denotes that the target domain samples are separable prior to adaptation to some extent but we can observe overlapped classes due to distributional gap between the two domains. Figure 2d denotes that SDAUP algorithm has aligned the source and the target distributions using the intermediate prototypical distribution.

For a class-level analysis, Figures 3a–3d visualize the confusion matrices for the classifier with explanations in the caption. We can see in Figure 3b that domain shift causes confusion between objects that are in visually similar classes, e.g., digits “3” and “8” or digits “4”, “7”, and “9”. Through SDAUP, the confusion is reduced for all classes, as seen in Figure 3c. Comparing Figure 3c with Figures 3a and 3d, we see that the initial confusions in the source domain translate into the easier target domain (Figures 3d) which is predictable from Theorem 1. Finally, Figure 3e depicts an empirical verification of Theorem 1. We observe that as more training iteration are performed and the distributions are aligned, the target domain testing accuracy constantly increases. This accords with Eq. (4) because SDAUP aligns the source domain distribution using the prototypical distribution.

7 Conclusions and Discussion

We addressed the sequential UDA problem. Our algorithm is based on minimizing the distributional domain discrepancy in a shared embedding space using an intermediate multi-modal prototypical distribution, modeled as a GMM. This distribution encodes what has been learned from the source domain. As a result, the classifier network that is trained in the source domain generalizes on the target domain. A future research direction is to overcome negative transfer for the source domain.

Broader Impact

Our sequential domain adaptation algorithm is quite general and potentially can be used to improve performance of machine learning systems after fielding these systems. Our algorithm is in particular helpful when preserving privacy of the original training dataset is necessary, e.g., healthcare datasets. Hence, this work can broaden the applicability of domain adaptation on more cases.

References

- [1] Mohammad Rostami, David Huber, and Tsai-Ching Lu. A crowdsourcing triage algorithm for geopolitical event forecasting. In *Proceedings of the 12th ACM Conference on Recommender Systems*, pages 377–381. ACM, 2018.
- [2] Xavier Glorot, Antoine Bordes, and Yoshua Bengio. Domain adaptation for large-scale sentiment classification: a deep learning approach. In *Proceedings of the 28th International Conference on International Conference on Machine Learning*, pages 513–520, 2011.
- [3] Hal Daumé III. Frustratingly easy domain adaptation. In *Proceedings of the 45th Annual Meeting of the Association of Computational Linguistics*, pages 256–263, 2007.
- [4] Mohammad Rostami. *Learning Transferable Knowledge Through Embedding Spaces*. PhD thesis, University of Pennsylvania, 2019.
- [5] Kaiming He, Xiangyu Zhang, Shaoqing Ren, and Jian Sun. Deep residual learning for image recognition. In *Proceedings of the IEEE Conference on Computer Vision and Pattern Recognition*, pages 770–778, 2016.
- [6] Swami Sankaranarayanan, Yogesh Balaji, Carlos D Castillo, and Rama Chellappa. Generate to adapt: Aligning domains using generative adversarial networks. In *Proceedings of the IEEE Conference on Computer Vision and Pattern Recognition*, pages 8503–8512, 2018.
- [7] Zhongyi Pei, Zhangjie Cao, Mingsheng Long, and Jianmin Wang. Multi-adversarial domain adaptation. In *Proceedings Thirty-Second AAAI Conference on Artificial Intelligence*, pages 3934–3941, 2018.
- [8] Yabin Zhang, Hui Tang, Kui Jia, and Mingkui Tan. Domain-symmetric networks for adversarial domain adaptation. In *Proceedings of the IEEE Conference on Computer Vision and Pattern Recognition*, pages 5031–5040, 2019.
- [9] Mingsheng Long, Zhangjie Cao, Jianmin Wang, and Michael I Jordan. Conditional adversarial domain adaptation. In *Advances in Neural Information Processing Systems*, pages 1640–1650, 2018.
- [10] Mingsheng Long, Yue Cao, Jianmin Wang, and Michael Jordan. Learning transferable features with deep adaptation networks. In *Proceedings of International Conference on Machine Learning*, pages 97–105, 2015.
- [11] Yaroslav Ganin and Victor Lempitsky. Unsupervised domain adaptation by backpropagation. In *Proceedings of International Conference on Machine Learning*, pages 1180–1189, 2015.
- [12] Mingsheng Long, Han Zhu, Jianmin Wang, and Michael I Jordan. Deep transfer learning with joint adaptation networks. In *Proceedings of the 34th International Conference on Machine Learning-Volume 70*, pages 2208–2217. JMLR. org, 2017.
- [13] Guoliang Kang, Lu Jiang, Yi Yang, and Alexander G Hauptmann. Contrastive adaptation network for unsupervised domain adaptation. In *Proceedings of the IEEE Conference on Computer Vision and Pattern Recognition*, pages 4893–4902, 2019.
- [14] Mohammad Rostami, Soheil Kolouri, Eric Eaton, and Kyungnam Kim. Deep transfer learning for few-shot sar image classification. *Remote Sensing*, 11(11):1374, 2019.
- [15] Mohammad Rostami, Soheil Kolouri, Praveen K Pilly, and James McClelland. Generative continual concept learning. In *AAAI*, pages 5545–5552, 2020.
- [16] Ian Goodfellow, Jean Pouget-Abadie, Mehdi Mirza, Bing Xu, David Warde-Farley, Sherjil Ozair, Aaron Courville, and Yoshua Bengio. Generative adversarial nets. In *Advances in Neural Information Processing Systems*, pages 2672–2680, 2014.

- [17] Kevin Roth, Aurelien Lucchi, Sebastian Nowozin, and Thomas Hofmann. Stabilizing training of generative adversarial networks through regularization. In *Advances in Neural Information Processing Systems*, pages 2018–2028, 2017.
- [18] Luke Metz, Ben Poole, David Pfau, and Jascha Sohl-Dickstein. Unrolled generative adversarial networks. In *International Conference on Learning Representations*, pages 1–14, 2017.
- [19] Baochen Sun and Kate Saenko. Deep coral: Correlation alignment for deep domain adaptation. In *European conference on computer vision*, pages 443–450. Springer, 2016.
- [20] Nicolas Courty, Rémi Flamary, Devis Tuia, and Alain Rakotomamonjy. Optimal transport for domain adaptation. *IEEE Transactions on Pattern Analysis and Machine Intelligence*, 39(9):1853–1865, 2016.
- [21] Bharath Bhushan Damodaran, Benjamin Kellenberger, Rémi Flamary, Devis Tuia, and Nicolas Courty. Deepjdot: Deep joint distribution optimal transport for unsupervised domain adaptation. In *Proceedings of the European Conference on Computer Vision (ECCV)*, pages 447–463, 2018.
- [22] Chen-Yu Lee, Tanmay Batra, Mohammad Haris Baig, and Daniel Ulbricht. Sliced wasserstein discrepancy for unsupervised domain adaptation. In *Proceedings of the IEEE Conference on Computer Vision and Pattern Recognition*, pages 10285–10295, 2019.
- [23] Mark Dredze and Koby Crammer. Online methods for multi-domain learning and adaptation. In *Proceedings of the Conference on Empirical Methods in Natural Language Processing*, pages 689–697. Association for Computational Linguistics, 2008.
- [24] V Jain and E Learned-Miller. Online domain adaptation of a pre-trained cascade of classifiers. In *Proceedings of the 2011 IEEE Conference on Computer Vision and Pattern Recognition*, pages 577–584, 2011.
- [25] Dongrui Wu. Online and offline domain adaptation for reducing bci calibration effort. *IEEE Transactions on Human-Machine Systems*, 47(4):550–563, 2016.
- [26] Yingwei Pan, Ting Yao, Yehao Li, Yu Wang, Chong-Wah Ngo, and Tao Mei. Transferrable prototypical networks for unsupervised domain adaptation. In *Proceedings of the IEEE Conference on Computer Vision and Pattern Recognition*, pages 2239–2247, 2019.
- [27] Chaoqi Chen, Weiping Xie, Wenbing Huang, Yu Rong, Xinghao Ding, Yue Huang, Tingyang Xu, and Junzhou Huang. Progressive feature alignment for unsupervised domain adaptation. In *Proceedings of the IEEE Conference on Computer Vision and Pattern Recognition*, pages 627–636, 2019.
- [28] N. Bonnotte. *Unidimensional and evolution methods for optimal transportation*. PhD thesis, Paris 11, 2013.
- [29] Y. Ganin, E. Ustinova, H. Ajakan, P. Germain, H. Larochelle, F. Laviolette, M. Marchand, and V. Lempitsky. Domain-adversarial training of neural networks. *The Journal of Machine Learning Research*, 17(1):2096–2030, 2016.
- [30] Eric Tzeng, Judy Hoffman, Kate Saenko, and Trevor Darrell. Adversarial discriminative domain adaptation. In *Proceedings of the IEEE Conference on Computer Vision and Pattern Recognition*, pages 7167–7176, 2017.
- [31] Muhammad Ghifary, W Bastiaan Kleijn, Mengjie Zhang, David Balduzzi, and Wen Li. Deep reconstruction-classification networks for unsupervised domain adaptation. In *European Conference on Computer Vision*, pages 597–613. Springer, 2016.
- [32] Alexander J Gabourie, Mohammad Rostami, Philip E Pope, Soheil Kolouri, and Kuyngnam Kim. Learning a domain-invariant embedding for unsupervised domain adaptation using class-conditioned distribution alignment. In *2019 57th Annual Allerton Conference on Communication, Control, and Computing (Allerton)*, pages 352–359, 2019.
- [33] Chao Chen, Zhihong Chen, Boyuan Jiang, and Xinyu Jin. Joint domain alignment and discriminative feature learning for unsupervised deep domain adaptation. In *Proceedings of the AAAI Conference on Artificial Intelligence*, volume 33, pages 3296–3303, 2019.
- [34] Konstantinos Bousmalis, George Trigeorgis, Nathan Silberman, Dilip Krishnan, and Dumitru Erhan. Domain separation networks. In *Advances in Neural Information Processing Systems*, pages 343–351, 2016.

- [35] Ming-Yu Liu and Oncel Tuzel. Coupled generative adversarial networks. In *Advances in neural information processing systems*, pages 469–477, 2016.
- [36] Saeid Motiian, Quinn Jones, Seyed Iranmanesh, and Gianfranco Doretto. Few-shot adversarial domain adaptation. In *Advances in Neural Information Processing Systems*, pages 6670–6680, 2017.
- [37] Judy Hoffman, Eric Tzeng, Taesung Park, Jun-Yan Zhu, Phillip Isola, Kate Saenko, Alexei Efros, and Trevor Darrell. CyCADA: Cycle-consistent adversarial domain adaptation. In *International Conference on Machine Learning*, pages 1989–1998, 2018.
- [38] Vivien Seguy, Bharath Bhushan Damodaran, Remi Flamary, Nicolas Courty, Antoine Rolet, and Mathieu Blondel. Large-scale optimal transport and mapping estimation. In *International Conference on Learning Representations*, 2018.
- [39] Pedro O Pinheiro. Unsupervised domain adaptation with similarity learning. In *Proceedings of the IEEE Conference on Computer Vision and Pattern Recognition*, pages 8004–8013, 2018.
- [40] Kuniaki Saito, Kohei Watanabe, Yoshitaka Ushiku, and Tatsuya Harada. Maximum classifier discrepancy for unsupervised domain adaptation. In *Proceedings of the IEEE Conference on Computer Vision and Pattern Recognition*, pages 3723–3732, 2018.
- [41] Leland McInnes, John Healy, Nathaniel Saul, and Lukas Großberger. UMAP: Uniform manifold approximation and projection. *Journal of Open Source Software*, 3(29):861, 2018.
- [42] A. Redko, I. and Habrard and M. Sebban. Theoretical analysis of domain adaptation with optimal transport. In *Joint European Conference on Machine Learning and Knowledge Discovery in Databases*, pages 737–753. Springer, 2017.
- [43] Fran ois Bolley, Arnaud Guillin, and C dric Villani. Quantitative concentration inequalities for empirical measures on non-compact spaces. *Probability Theory and Related Fields*, 137(3-4):541–593, 2007.

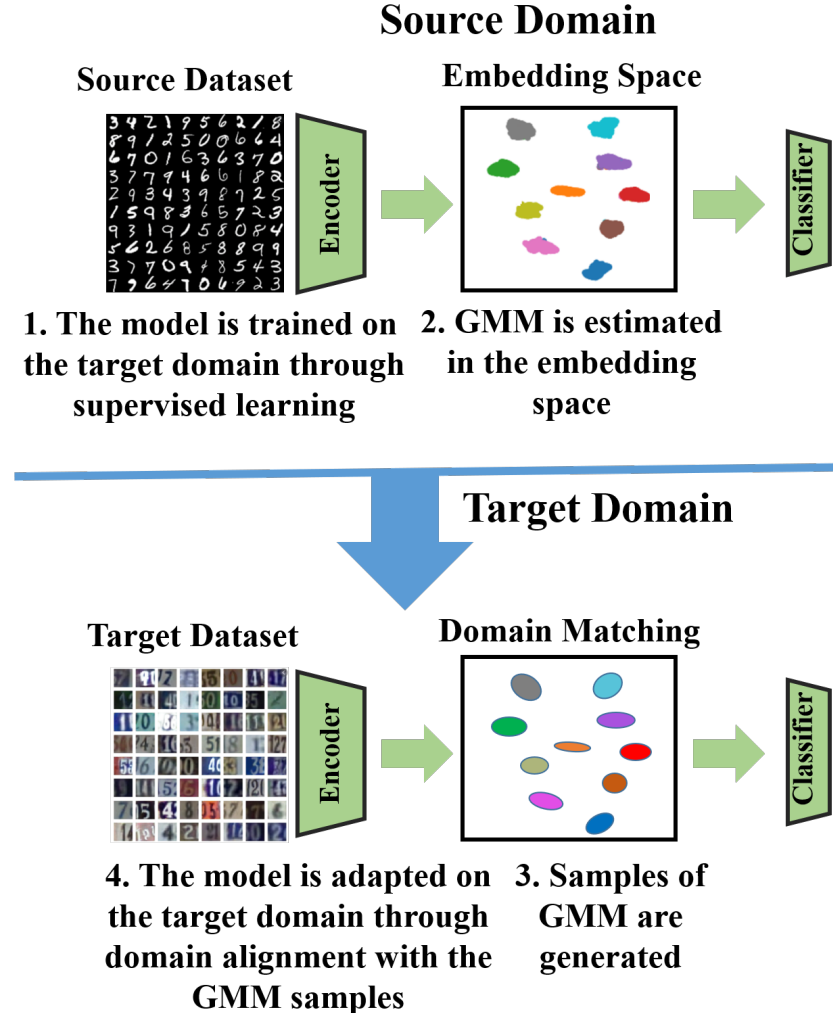


Figure 4: Architecture of the proposed sequential unsupervised domain adaptation framework.

A Block Diagram of the Proposed Method

Figure 4 presents an enlarged version of the system block-diagram for more clarity. Visualization of the data representation in the embedding space in Figure 4, to highlights formation of a multi-modal distribution when the model is trained on the source domain (MNIST dataset in this Figure). We can fit this distribution with a GMM distribution and the number of components of this GMM is equal to the number of classes. After having a trained model, we update the model to generalize well on the target domain (SVHN dataset in this Figure).

B Proof of Theorem 1

We first note that When we generate the pseudo-dataset, we ensure to select pseudo-data points for which the model is confident. To this end, we pick a threshold τ , draw random pseudo-data points z_i^p , and pass them through the classifier sub-network. We then look at the predicted label distribution at the final softmax layer and include only those data-points for which the model is confident with prediction probability greater than τ . Let e_P denotes the true risk of the initial optimal model that is trained using the source on the generated pseudo-dataset.

Our proof is based on the following theorem by Redko et al. [42] and using a result by Bolley [43] which measure the convergence of the empirical distribution to the true distribution in terms of the WD distance.

Theorem 2 (Redko et al. [42]): Under the assumptions described in our framework, assume that a model is trained on the source domain, then for any $d' > d$ and $\zeta < \sqrt{2}$, there exists a constant number N_0 depending on d' such that for any $\xi > 0$ and $\min(N, M) \geq \max(\xi^{-(d'+2)}, 1)$ with probability at least $1 - \xi$, the following holds:

$$e_{\mathcal{T}} \leq e_{\mathcal{S}} + W(\hat{\mu}_{\mathcal{T}}, \hat{\mu}_{\mathcal{S}}) + e_C(\mathbf{w}^*) + \sqrt{(2 \log(\frac{1}{\xi})/\zeta)} \left(\sqrt{\frac{1}{N}} + \sqrt{\frac{1}{M}} \right). \quad (5)$$

Theorem 2 provides an upperbound for the performance of the source domain trained model on the target domain. We use Theorem 2 to deduce Theorem 1. Redko et al. [42] prove Theorem 2 for a binary classification setting in a joint training UDA setting. We also provide our proof in this case but it can be conveniently extended.

Theorem 1 : Consider that we generate a pseudo-dataset using the prototypical distribution and update the model for sequential UDA using SDAUP algorithm. Then, the following holds:

$$e_{\mathcal{T}} \leq e_{\mathcal{S}} + W(\hat{\mu}_{\mathcal{S}}, \hat{\mu}_{\mathcal{P}}) + W(\hat{\mu}_{\mathcal{T}}, \hat{\mu}_{\mathcal{P}}) + (1 - \tau) + e_{C'}(\mathbf{w}^*) + \sqrt{(2 \log(\frac{1}{\xi})/\zeta)} \left(\sqrt{\frac{1}{N}} + \sqrt{\frac{1}{M}} + 2\sqrt{\frac{1}{N_p}} \right), \quad (6)$$

where ξ is a constant which depends on $\mathcal{L}(\cdot)$ and $e'_C(\mathbf{w}^*)$ denotes the expected risk of the optimally joint trained model when used on both the source domain and the pseudo-dataset.

Proof: Since the parameter τ denotes the performance of the source-trained model on the pseudo-data points in the embedding space, then the probability that the predicted labels for the pseudo-data points to be false by this model is equal to $1 - \tau$. We can define the following difference for the pseudo-data points:

$$|\mathcal{L}(h_{\mathbf{w}_0}(\mathbf{z}_i^p), \mathbf{y}_i^p) - \mathcal{L}(h_{\mathbf{w}_0}(\mathbf{z}_i^p), \hat{\mathbf{y}}_i^p)| = \begin{cases} 0, & \text{if } \mathbf{y}_i^p = \hat{\mathbf{y}}_i^p. \\ 1, & \text{otherwise.} \end{cases} \quad (7)$$

Hence, the expectation on the above error can be computed as:

$$\mathbb{E}(|\mathcal{L}(h_{\mathbf{w}_0}(\mathbf{z}_i^p), \mathbf{y}_i^p) - \mathcal{L}(h_{\mathbf{w}_0}(\mathbf{z}_i^p), \hat{\mathbf{y}}_i^p)|) \leq |e_{\mathcal{P}} - e_{\mathcal{T}}| \leq (1 - \tau). \quad (8)$$

Using Eq. (8) we can deduce:

$$e_{\mathcal{S}} + e_{\mathcal{T}} = e_{\mathcal{S}} + e_{\mathcal{T}} + e_{\mathcal{P}} - e_{\mathcal{P}} \leq e_{\mathcal{S}} + e_{\mathcal{P}} + |e_{\mathcal{T}} - e_{\mathcal{P}}| \leq e_{\mathcal{S}} + e_{\mathcal{P}} + (1 - \tau). \quad (9)$$

Note that since Eq. (9) is valid for all \mathbf{w} , if we consider the joint optimal parameter \mathbf{w}^* in the right-hand and the left-hand sides of Eq. (9), we deduce:

$$e_C(\mathbf{w}^*) \leq e'_C(\mathbf{w}) + (1 - \tau). \quad (10)$$

Now by considering Theorem 2 for the two domains and then applying Eq. (10) on Eq.(5), we have:

$$e_{\mathcal{T}} \leq e_{\mathcal{S}} + W(\hat{\mu}_{\mathcal{T}}, \hat{\mu}_{\mathcal{S}}) + e'_C(\mathbf{w}^*) + (1 - \tau) + \sqrt{(2 \log(\frac{1}{\xi})/\zeta)} \left(\sqrt{\frac{1}{N}} + \sqrt{\frac{1}{M}} \right). \quad (11)$$

Now using the triangular inequality on the WD metric we can deduce:

$$W(\hat{\mu}_{\mathcal{T}}, \hat{\mu}_{\mathcal{S}}) \leq W(\hat{\mu}_{\mathcal{T}}, \hat{\mu}_{\mathcal{P}}) + W(\hat{\mu}_{\mathcal{S}}, \hat{\mu}_{\mathcal{P}}) \leq W(\hat{\mu}_{\mathcal{T}}, \hat{\mu}_{\mathcal{P}}) + W(\hat{\mu}_{\mathcal{S}}, \hat{\mu}_{\mathcal{P}}) + 2W(\hat{\mu}_{\mathcal{P}}, \hat{\mu}_{\mathcal{P}}). \quad (12)$$

Now we simplify the term $W(\hat{\mu}_{\mathcal{P}}, \hat{\mu}_{\mathcal{P}})$ using Theorem 1.1 in the work by Bolley et al. [43].

Theorem 3 (Theorem 1.1 by Bolley et al. [43]): consider that $p(\cdot) \in \mathcal{P}(\mathcal{Z})$ and $\int_{\mathcal{Z}} \exp(\alpha \|\mathbf{x}\|_2^2) dp(\mathbf{x}) < \infty$ for some $\alpha > 0$. Let $\hat{p}(\mathbf{x}) = \frac{1}{N} \sum_i \delta(\mathbf{x}_i)$ denote the empirical distribution that is built from the samples $\{\mathbf{x}_i\}_{i=1}^N$ that are drawn i.i.d from $\mathbf{x}_i \sim p(\mathbf{x})$. Then for any $d' > d$ and $\xi < \sqrt{2}$, there exists N_0 such that for any $\epsilon > 0$ and $N \geq N_0 \max(1, \epsilon^{-(d'+2)})$, we have:

$$P(W(p, \hat{p}) > \epsilon) \leq \exp\left(-\frac{-\xi}{2} N \epsilon^2\right) \quad (13)$$

This relation measure the distance between the estimated empirical distribution and the true distribution in terms of the WD distance.

Applying Eq. (12) and Eq. (13) on Eq. (11) concludes Theorem 2 as stated:

$$e_{\mathcal{T}} \leq e_{\mathcal{S}} + W(\hat{\mu}_{\mathcal{S}}, \hat{\mu}_{\mathcal{P}}) + W(\hat{\mu}_{\mathcal{T}}, \hat{\mu}_{\mathcal{P}}) + (1 - \tau) + e_{C'}(\mathbf{w}^*) + \sqrt{(2 \log(\frac{1}{\xi})/\zeta)} \left(\sqrt{\frac{1}{N}} + \sqrt{\frac{1}{M}} + 2\sqrt{\frac{1}{N_p}} \right), \quad (14)$$

C Details of Experimental Implementation

In the digit recognition experiments, we resized the images of SVHN dataset to 28×28 images to have the same size of the MNIST and the USPS datasets. This is necessary because we use the same encoder across all domains.

In our experiments, we used cross entropy loss as the discrimination. At each training epoch, we computed the loss function and stop training when the loss function became constant. We used Keras for implementation and ADAM optimizer. We tune the learning rate such that the loss function reduces smoothly. We run our code on a cluster node equipped with 2 Nvidia Tesla P100-SXM2 GPU's.

All the datasets have their own standard training/testing splits in all domains. For each experiment, we used these testing splits to measure performance of the methods that we report in terms of classification accuracy. We used the classification rate on the testing set to measure performance of the algorithms. We performed 10 training trials and reported the average performance and the standard deviation on the testing sets for these trials.